

Research on hydrodynamic performance calculation of buoy-chain-sprocket wave energy collection device

Pengfei Fang, Xiangdong Su, Deshuai Chen and Linsen Zhu*

Research Center of Mechanics and Mechatronic Equipment, Shandong University
Weihai, China

*Corresponding author e-mail: zllinsen@sdu.edu.cn

Abstract. Buoy-chain-sprocket wave energy collection device is a new type of oscillating buoy wave energy collection device, which has a good application prospect. The calculation method of the hydrodynamic performance of wave energy device (e.g. the first-level average collection efficiency of wave energy) is the core scientific problem of wave energy device, and it is also the theoretical basis for the optimization and control of wave energy device prototype. In this paper, on basis of linear potential flow theory, after the velocity potentials are calculated with eigenfunction expansion method and matching asymptotic expansion method, the frequency-domain wave loads in the heave, surge and pitch directions of the floating body are obtained. And then the motion coordination relationship of the floating body of buoy-chain-sprocket wave energy collection device is used to establish time-domain hydrodynamic motion response equations of the floating body of the device based on the Cummins method. After these equations are solved via the fourth-order Runge-Kutta method, the first-level average collection efficiency of the wave energy device is acquired. In order to further improve the calculation accuracy, the frequency-domain wave-exciting force is calculated by using variable draft depth when the hydrodynamic response of buoy-chain-sprocket wave energy collection device is calculated in this paper. Finally, the reliability of the above calculation method for the hydrodynamic performance of buoy-chain-sprocket wave energy collection device is verified through physical model experiment.

Keywords: wave energy; time-domain analysis; hydrodynamic response; hydrodynamic performance; Cummins method.

1. Introduction

Wave energy is a clean and renewable energy in the ocean, with the advantages of high energy flow density, large reserves, and wide distribution [1, 2], and its exploitation and utilization technology has been paid attention by coastal countries around the world increasingly [3, 4]. Among various wave energy utilization technologies, oscillating buoy wave energy collection technology has become a research hotspot in the field of wave energy utilization due to its advantages of simple device structure, good reliability, low operation and maintenance cost, and high collection efficiency.

Currently, the wave energy utilization technology in the world has not been put into application widely, and the main reason is that it is restricted by the reliability and economy of the existing wave energy utilization technology [5]. Buoy-chain-sprocket wave energy utilization technology is proposed by Shandong University [6, 7], belonging to the oscillating buoy wave energy collection technology. The buoy-chain-sprocket mechanism is used to collect wave energy in this technology with good application prospects. The calculation method of hydrodynamic performance of wave energy device is one of core scientific problems of wave energy utilization technology. On basis of on linear potential flow theory, this paper intends to study the hydrodynamic performance calculation method of buoy-chain-sprocket wave energy collection device by means of combining theoretical calculation research and physical model experiment research, so as to provide a theoretical basis for the optimization and control of the device prototype in the future.

2. Working principle of buoy-chain-sprocket wave energy collection device

As shown in Fig. 1, buoy-chain-sprocket wave energy collection device is primarily made up of a cylindrical floating body, sprocket, chain, conduit, guide rod, anchor chain, gravity anchor, hydraulic cylinder, and hydraulic power generation system. With the effect of the wave force, a pitching motion around the spherical joint and an oscillating motion along the guide rod are main motions that the floating body of the device produces. During the rising stage of the floating body along the guide rod, the piston rod of the hydraulic cylinder is pulled by the chain through the sprocket group, and then high-pressure oil is generated via the hydraulic cylinder. After being buffered by the accumulator, the hydraulic motor driven by the oil rotates, and then the generator driven via the hydraulic motor generates electricity. During the descending stage of the floating body along the guide rod, with the piston rod reset under the effect of low-pressure oil, chain is recovered, so one-way wave energy collection is a feature of buoy-chain-sprocket wave energy collection device. Approximately constant damping force, as well as approximately constant chain retraction force, is the feature of the first-level wave energy collection process of the device, for the pressure at the outlet and inlet of the hydraulic cylinder holds changeless.

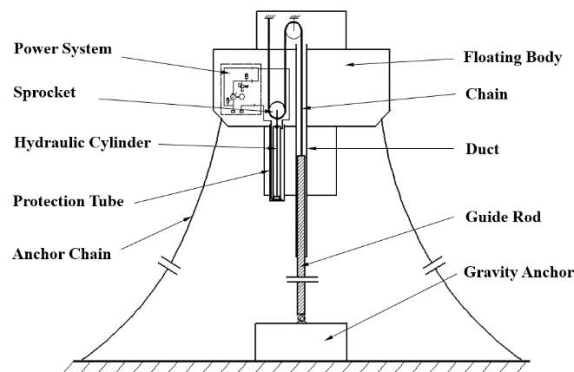


Fig. 1 Schematic of the buoy-chain-sprocket wave energy collection device.

Under the effect of regular waves, the motion of the floating body of the device can be simplified as two degrees of freedom motion. One is pitching motion around the spherical joint and the other is oscillating motion along the guide rod. However, in this paper, the motion of the floating body is described with three motions: heave, surge, and pitch, as shown in Fig. 2, so as to facilitate the description of the velocity potential. And then the kinematic coordination relationship is used to constrain these three motions, seen from (1) ~ (9), so that the three-degree-of-freedom motion can be converted into a two-degree-of-freedom motion.

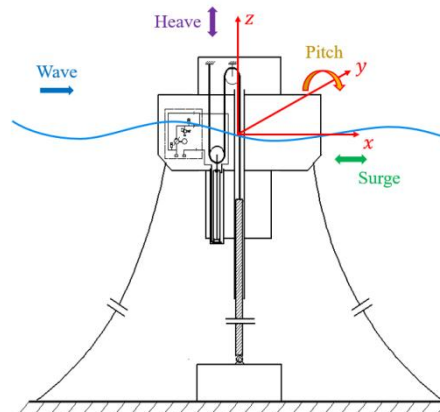


Fig. 2 The motion diagram of buoy-chain-sprocket wave energy collection device.

3. Mathematical model

3.1 Kinematic Analysis

In Fig. 3, the coordinate system oxz is fixed on the still water surface. The coordinate system $o_0x_0z_0$ is fixed on the floating body, swaying with the floating body at all times and coinciding with the coordinate system oxz when the floating body is in the hydrostatic equilibrium position. The coordinate system $o'x'z'$ whose origin always coincides with the origin of the coordinate system $o_0x_0z_0$, absolutely coincides with the coordinate system oxz when the floating body is in the hydrostatic equilibrium position, and its axes are respectively parallel to the corresponding axes of the coordinate system oxz at other positions.

Based on Chasles theorem, taking the point o_0 on the floating body as the base point, the motion of each point on the floating body in plane motion can be described as the composition of two motions, respectively the translation with the base point o_0 and the rotation around the axis that passes through the base point o_0 and is parallel to the axis y . In Fig. 3, $\overline{o_0o}$ represents the translational displacement of the point o_0 on the floating body in the coordinate system oxz . The translational displacement of the point o_0 on the x axis and z axis in the coordinate system oxz are denoted as $x(t)$ and $z(t)$ respectively. The relative displacement of the floating body along the axis of the guide rod is expressed by $l(t)$. θ represents the angular displacement of the floating body rotating around the base point o_0 , which is equal to the angular displacement of the floating body rotating around the point p . Compared with the water depth h_0 , the height of the gravity anchor is too small so that the distance between point o and point p is regarded as h_0 .

According to Fig. 3, the kinematic relationship is established, shown as (1) ~ (9), which contain the coordination relationship among the heave, surge, and pitch motions of the floating body.

$$z(t) = (h_0 + l(t)) \cos \theta - h_0 \tag{1}$$

$$x(t) = (h_0 + l(t)) \sin \theta \tag{2}$$

$$v_l = \frac{dl(t)}{dt} \tag{3}$$

$$a_l = \frac{dv_l}{dt} \tag{4}$$

$$\ddot{\theta} = \frac{d\dot{\theta}}{dt} \tag{5}$$

$$v_z = \frac{dz(t)}{dt} = v_l \cos \theta - (h_0 + l(t)) \sin \theta \cdot \dot{\theta} \tag{6}$$

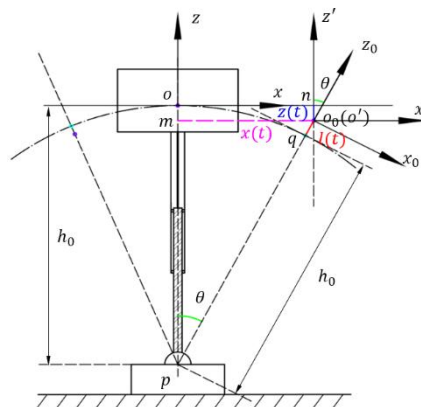


Fig. 3 Schematic diagram of the kinematic relationship of the device.

$$a_z = \frac{dv_z}{dt} = a_l \cos \theta - 2v_l \sin \theta \cdot \dot{\theta} - (h_0 + l(t)) \cos \theta \cdot (\dot{\theta})^2 - (h_0 + l(t)) \sin \theta \cdot \ddot{\theta} \tag{7}$$

$$v_x = \frac{dx(t)}{dt} = v_l \sin \theta + (h_0 + l(t)) \cos \theta \cdot \dot{\theta} \tag{8}$$

$$a_x = \frac{dv_x}{dt} = a_l \sin \theta + 2v_l \cos \theta \cdot \dot{\theta} - (h_0 + l(t)) \sin \theta \cdot (\dot{\theta})^2 + (h_0 + l(t)) \cos \theta \cdot \ddot{\theta} \tag{9}$$

3.2 Force Analysis

After analyzing the force of the guide rod, its schematic diagram of the force analysis is acquired, as shown in Fig. 4.

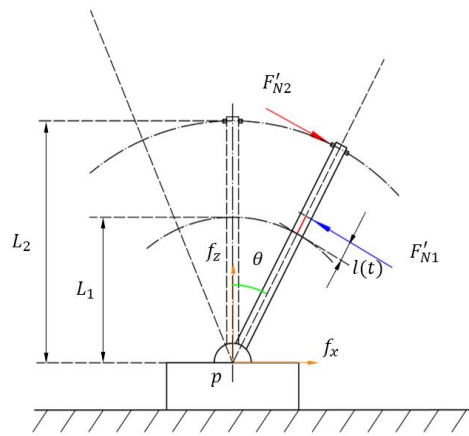


Fig. 4 Schematic diagram of the force analysis of the guide rod.

Since the guide rod and the gravity anchor are hinged at the point p , there is no moment. During the movement of the floating body, there are two forces perpendicular to the guide rod. They are at both ends of the part where the duct and the guide rod overlap (the contact part between the guide rod and the duct fixed at the bottom of the floating body). And the frictional force at these two places is relatively small and can be ignored due to the guide wheels at these two places. Therefore, the force of the guide rod at these two places can be denoted as F'_{N1} and F'_{N2} respectively, as shown in Fig. 4. Ignoring the rotational inertia of the guide rod, the moment balance formula is established as (10).

$$F'_{N2}L_2 - F'_{N1}(L_1 + l(t)) = 0 \tag{10}$$

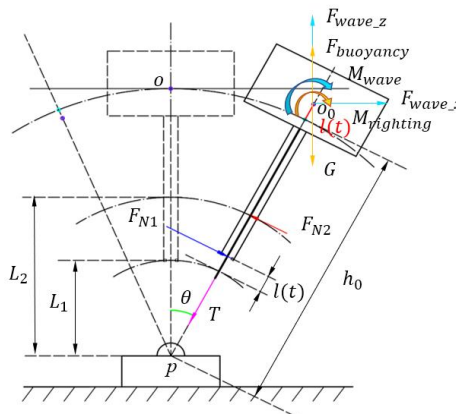


Fig. 5 Schematic diagram of the force analysis of the floating body.

Subsequently, the force analysis for the floating body is carried out, and its schematic diagram is shown in Fig. 5. Since F_{N1} and F'_{N1} , as well as F_{N2} and F'_{N2} , are a pair of interaction forces, we gain (11).

$$F_{N2}L_2 - F_{N1}(L_1 + l(t)) = 0 \tag{11}$$

The component forces of the wave force F_{wave} on the x axis and z axis of the floating body are respectively expressed by F_{wave_x} and F_{wave_z} . The wave force F_{wave} consisting of two parts, the first part is wave-exciting force, and the second part is wave force formed by radiation effect. When solving wave-exciting force, the effect of the shape of the floating body on the incident field is considered. Affected by the floating body, a scattered field will be formed around the floating body in the incident field. The other part of the wave force F_{wave} reflects the reaction force of the wave due to the movement of the floating body around which a radiation field is formed. M_{wave} is composed of the wave-exciting moment and the wave reaction moment received by the moving floating body. The buoyancy and gravity on the floating body are denoted as $F_{buoyancy}$ and G respectively. $M_{righting}$ is the hydrostatic restoring moment on the floating body.

T represents the tension on the chain, which satisfies

$$T = F_{damping} + F_{chain-retraction} \tag{12}$$

where $F_{damping}$ is the damping force of PTO (Power Take-Off) system of the device, and $F_{chain-retraction}$ represents the chain retraction force. The hydraulic cylinder is used to provide the chain retraction force for the device studied in this paper.

3.3 Dynamic Equation

One of the keys to establishing dynamic equation is the calculation of wave load. In this paper, time domain analysis is carried out based on Cummins method [8]. The time-domain dynamic equation is

$$\begin{aligned} & \sum_{j=1}^3 \{ (M_{(2k-1)(2j-1)} + m_{(2k-1)(2j-1)}) \ddot{\xi}_{(2j-1)}(t) \\ & + \int_{-\infty}^t \dot{\xi}_{(2j-1)}(\tau) K_{(2k-1)(2j-1)}(t-\tau) d\tau + B_{(2k-1)}[\dot{\xi}_{(2j-1)}(t)] \\ & + C_{(2k-1)(2j-1)} \xi_{(2j-1)}(t) \} = F_{(2k-1)}(t) - F_{other(2k-1)}(t), \end{aligned} \tag{13}$$

$(k = 1, 2, 3)$

where $M_{(2k-1)(2j-1)}$ is the generalized mass of the floating body, $m_{(2k-1)(2j-1)}$ is the time-domain added mass of the floating body, $K_{(2k-1)(2j-1)}(t-\tau)$ is the hysteresis function, $B_{(2k-1)}[\dot{\xi}_{(2j-1)}(t)]$ is the viscous damping of the system, $C_{(2k-1)(2j-1)}$ is the hydrostatic restoring force coefficient, $F_{(2k-1)}(t)$ is the time-domain wave-exciting force on the floating body, and $F_{other(2k-1)}(t)$ is external force received by the floating body from the chain and guide rod.

In this method, the time-domain wave loads are calculated based on the frequency-domain wave loads. Time-domain wave-exciting force $F_{(2k-1)}(t)$ on the floating body can be obtained by inverse Fourier transform of the linear transfer function $H_{(2k-1)}(\omega)$ acquired in the frequency domain and convolution with the wave surface function $\eta(\tau)$, as shown as (14) and (15), where $H_{(2k-1)}(\omega)$ is the

first-order frequency-domain wave-exciting force of the floating body with the effect of unit amplitude regular waves.

$$F_{(2k-1)}(t) = \int_{-\infty}^t h_{(2k-1)}(t-\tau)\eta(\tau)d\tau, \quad (k=1,2,3) \quad (14)$$

$$h_{(2k-1)}(t) = \text{Re} \left\{ \frac{1}{\pi} \int_0^{\infty} H_{(2k-1)}(\omega) e^{i\omega t} d\omega \right\} \quad (15)$$

The hysteresis function is able to be obtained by inverse Fourier transform of the frequency-domain radiation damping $b_{(2k-1)(2j-1)}$. The equation is as follows.

$$K_{(2k-1)(2j-1)}(t) = \frac{2}{\pi} \int_0^{\infty} b_{(2k-1)(2j-1)}(\omega) \cos(\omega t) d\omega \quad (16)$$

The time-domain added mass can be obtained according to the following equation.

$$m_{(2k-1)(2j-1)} = a_{(2k-1)(2j-1)}(\infty) \quad (17)$$

3.3.1 Calculation of $H_{(2k-1)}(\omega)$, $a_{(2k-1)(2j-1)}$ and $b_{(2k-1)(2j-1)}$.

Since the shape of the floating body of buoy-chain-sprocket wave energy collection device is similar to a cylinder, based on potential flow theory, the velocity potential can be efficiently solved by using eigenfunction expansion method and matching asymptotic expansion method [9, 10]. Subsequently, the frequency-domain wave-exciting force, frequency-domain added mass, and frequency-domain radiation damping of the floating body can be obtained by using Bernoulli equation.

On basis of potential flow theory, the idea of solving velocity potential in the frequency domain is to decompose the velocity potential of flow field into incident velocity potential, scattering velocity potential, and radiation velocity potential, which are respectively used to characterize incident effect, scattering effect and radiation effect in the process of wave and floating body interaction. Each velocity potential with the same governing equation and different boundary condition equations, is solved respectively. In addition, when solving velocity potential in the frequency domain, it is generally considered that velocity potential can be separated as spatial and temporal components, so as to simplify the solution of the velocity potential. The relationship between velocity potential Φ and φ is

$$\Phi = \text{Re}(\varphi \cdot e^{-i\omega t}) \quad (18)$$

The coordinate system is established, as shown in Fig. 6. And then the solution conditions of each velocity potential are presented as follows.

The governing equation and boundary condition equations satisfied by the incident velocity potential are

$$\nabla^2 \varphi_I = 0 \quad (19)$$

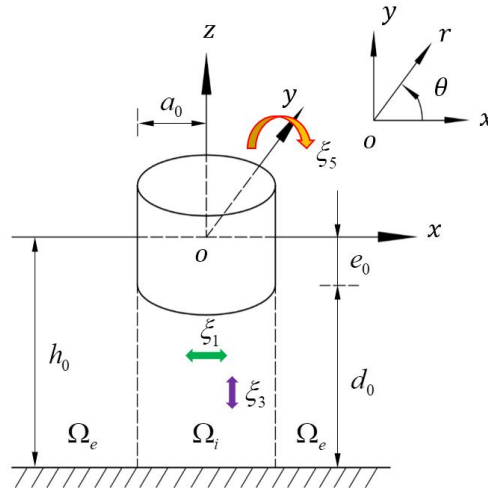


Fig. 6 Schematic diagram of coordinate system and fluid field division.

$$\frac{\partial \varphi_I}{\partial z} - \frac{\omega^2}{g} \varphi_I = 0, \quad (z = 0) \tag{20}$$

$$\frac{\partial \varphi_I}{\partial z} = 0, \quad (z = -h_0) \tag{21}$$

The governing equation and boundary condition equations satisfied by the scattering velocity potential are

$$\nabla^2 \varphi_D = 0 \tag{22}$$

$$\frac{\partial \varphi_D}{\partial z} - \frac{\omega^2}{g} \varphi_D = 0, \quad (z = 0) \tag{23}$$

$$\frac{\partial \varphi_D}{\partial z} = 0, \quad (z = -h_0) \tag{24}$$

$$\frac{\partial \varphi_D}{\partial n} = -\frac{\partial \varphi_I}{\partial n}, \quad (r = a_0, -e_0 \leq z \leq 0 \cup z = -e_0, 0 \leq r \leq a_0) \tag{25}$$

$$\lim_{r \rightarrow \infty} \sqrt{r} \left(\frac{\partial \varphi_D}{\partial r} - ik \varphi_D \right) = 0 \tag{26}$$

In this paper, the radiation velocity potential is composed of surge, heave, and pitch motion modes radiation velocity potential. If the velocity potentials aroused by the unit amplitude motion of the floating body under each motion mode are denoted as $\phi_{(2k-1)}$, $k = 1, 2, 3$, we will get

$$\varphi_R = \sum_{k=1}^3 \xi_{(2k-1)} \phi_{(2k-1)} \tag{27}$$

The governing equations and boundary condition equations satisfied by the radiation velocity potential are

$$\nabla^2 \varphi_R = 0 \tag{28}$$

$$\frac{\partial \varphi_R}{\partial z} - \frac{\omega^2}{g} \varphi_R = 0, \quad (z = 0) \tag{29}$$

$$\frac{\partial \varphi_R}{\partial z} = 0, \quad (z = -h_0) \tag{30}$$

$$\frac{\partial \varphi_R}{\partial n} = -i\omega \sum_{k=1}^3 \xi_{(2k-1)}^e n_{(2k-1)}, \quad (r = a_0, -e_0 \leq z \leq 0 \cup z = -e_0, 0 \leq r \leq a_0) \tag{31}$$

$$\lim_{r \rightarrow \infty} \sqrt{r} \left(\frac{\partial \varphi_R}{\partial r} - ik \varphi_R \right) = 0 \tag{32}$$

For a cylindrical floating body, the key to solving velocity potentials by using eigenfunction expansion method and matching asymptotic expansion method, is to construct velocity potentials with eigenfunctions which satisfy velocity potentials conditions of the interior region Ω_i and exterior region Ω_e respectively, and also satisfy continuous conditions shown as (33) and (34). The continuous conditions are built, for the velocity potential, as well as the velocity of fluid, is same at the connection between exterior region and interior region. The exterior region and interior region velocity potentials are obtained, after solving the undetermined coefficients of φ_i and φ_e .

$$\varphi_e(r, \theta, z) = \varphi_i(r, \theta, z), \quad (r = a_0, -h_0 \leq z \leq -e_0) \tag{33}$$

$$\frac{\partial}{\partial r} \varphi_e(r, \theta, z) = \frac{\partial}{\partial r} \varphi_i(r, \theta, z), \quad (r = a_0, -h_0 \leq z \leq -e_0) \tag{34}$$

After obtaining velocity potential, $H_{(2k-1)}(\omega)$ is obtained according to (35) and (36). $a_{(2k-1)(2j-1)}(\omega)$ and $b_{(2k-1)(2j-1)}(\omega)$ are obtained according to (37).

$$H_{(2k-1)}(\omega) = \iint_S i\omega \rho (\varphi_i + \varphi_D) n_{(2k-1)} ds, \quad (k = 1, 2, 3) \tag{35}$$

$$[n_1, n_3, n_5] = [n_x, n_z, zn_x - xn_z] \tag{36}$$

$$a_{(2k-1)(2j-1)} + i \frac{b_{(2k-1)(2j-1)}}{\omega} = \rho \iint_S \phi_{(2j-1)} n_{(2k-1)} ds, \quad (k = 1, 2, 3, j = 1, 2, 3) \tag{37}$$

Since it is similar to use eigenfunction expansion method and matching asymptotic expansion method to solve velocity potentials mentioned above, taking radiation velocity potential as an example, the reliability of our codes based on Matlab for frequency domain calculation is verified via respectively comparing the added mass and radiation damping with a classical literature [9] under the same conditions. The comparison is shown in Fig. 7.

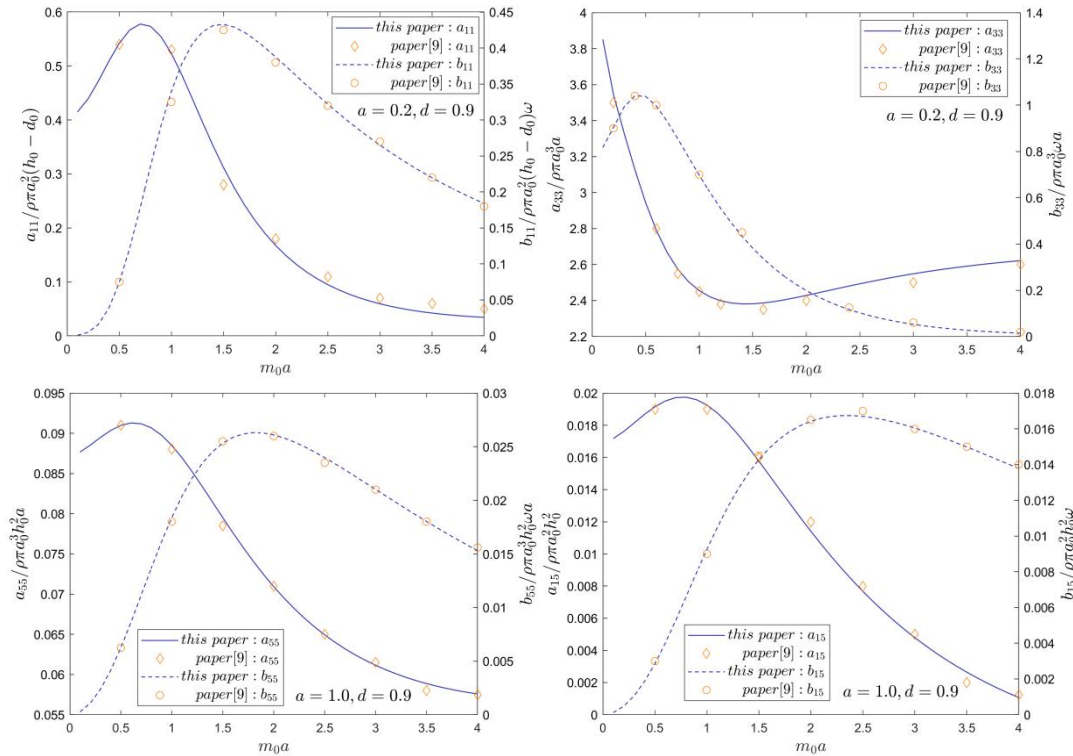


Fig. 7 Comparison of numerical results of added mass and radiation damping.

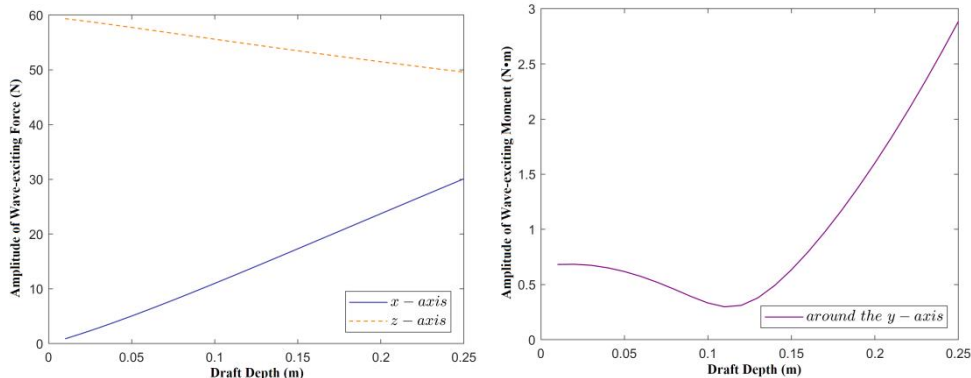


Fig. 8 Relationship between the amplitude of wave-exciting force and draft depth of the floating body.

When calculating the time-domain wave-exciting force $F_{(2k-1)}(t)$ based on (14) and (15), the frequency-domain wave-exciting force $H_{(2k-1)}(\omega)$ is used, whose amplitude is related to the draft depth of the floating body. Take the wave conditions of the physical model experiment in Table 2 as an example, its amplitude varies with the draft depth of the floating body as shown in Fig. 8. It can be seen from Fig. 8 that its amplitude varies greatly with the draft depth of the floating body. In order to improve the calculation accuracy, we respectively use the average draft depth and varying draft depth of the floating body to calculate the frequency-domain wave-exciting force, and then compare time-domain hydrodynamic responses of the device based on these two calculation methods toward the frequency-domain wave-exciting force. These two time-domain hydrodynamic responses are denoted as the results based on method 1 and method 2 respectively.

3.3.2 Calculation of $F_{other(2k-1)}(t)$. According to the force analysis, we can get

$$F_{other(2k-1)}(t) = T \sin \theta - (F_{N1} + F_{N2}) \cos \theta, \quad (k = 1)$$

$$F_{other (2k-1)}(t) = T \cos \theta + (F_{N1} + F_{N2}) \sin \theta, \quad (k = 2)$$

$$F_{other (2k-1)}(t) = F_{N1}(h_0 - L_1) + F_{N2}(h_0 - L_2 + l(t)), \quad (k = 3) \quad (38)$$

3.4 Numerical Calculation Method of Dynamic Equation

When solving the three coupled time-domain second-order differential equations (included in (13)), the fourth-order Runge-Kutta method is used for time discretion. At current time step, only a_z , a_x , $\ddot{\theta}$, F_{N1} , and F_{N2} are unknown. For a_z and a_x can be represented by a_l according to (7) and (9), only a_l , $\ddot{\theta}$, F_{N1} , and F_{N2} are unknown at current time step. Combining (11) and (13), and four unknown quantities can be solved by these four equations. The parameters such as velocity and displacement at the current time step are obtained from the previous time step according to the definitions of acceleration and velocity, and the velocity and displacement of the initial time step are obtained according to the initial conditions.

3.5 Calculation Method of Device Performance

The calculation formula of the first-level instantaneous collection power of the device is

$$P(t) = T(t) \times v_l(t) \quad (39)$$

The calculation formula of the first-level average collection power of the device is

$$\bar{P} = \frac{1}{T} \int_{t_1}^{t_1+T} P(t) dt \quad (40)$$

where t_1 can be chosen arbitrarily when the device is in a stable periodic motion state.

The calculation formula of the first-level average collection efficiency of the device is

$$\eta = \frac{\bar{P}}{\bar{P}_{wave}} \times 100\% \quad (41)$$

where \bar{P}_{wave} is

$$\bar{P}_{wave} = \left[\frac{1}{16} \rho g H^2 \frac{\omega}{k} \left(1 + \frac{2kh_0}{\sinh 2kh_0} \right) \right] \times 2a_0 \quad (42)$$

where ρ is fluid density, g is gravitational acceleration, H is wave height, k is wave number, ω is wave frequency, h_0 is water depth, and a_0 is the radius of floating body. The wave number k is calculated using the dispersion relation of wave.

4. Physical model experiment

In order to verify the reliability of the hydrodynamic performance calculation method of buoy-chain-sprocket wave energy collection device, we carry out a physical model experimental study.

4.1 Physical Model Experimental Platform

The model test platform of buoy-chain-sprocket wave energy collection device consists of five parts: wave height meter, wave tank, plunger type wave generator, dam to eliminate waves, and the wave energy collection physical model device. The schematic diagram is shown in Fig. 9. The synchronous belt goes around the synchronous pulley, one end is connected with the constant force

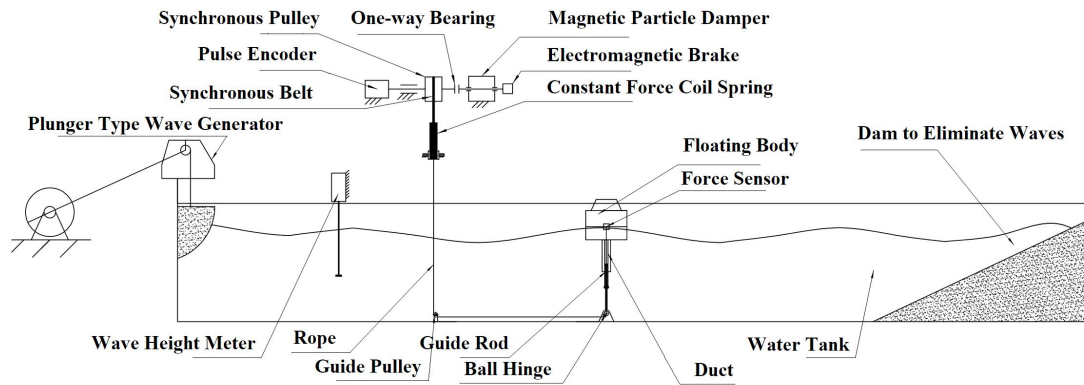


Fig. 9 Schematic diagram of the indoor physical model experiment platform of buoy-chain-sprocket wave energy collection device.

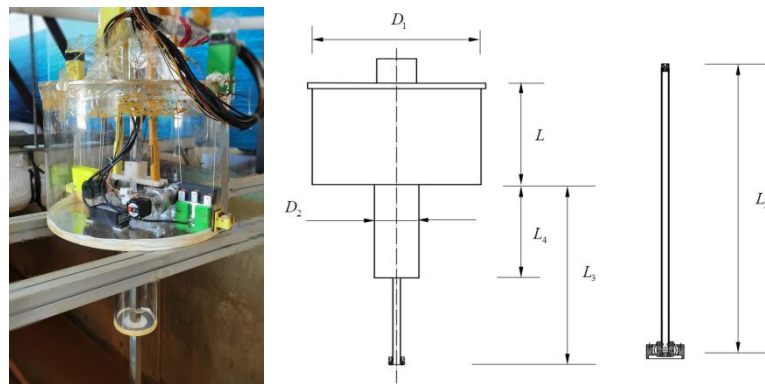


Fig. 10 The floating body and guide rod of the physical model.

Table 1. Main parameters of the prototype and physical model

	Mass (kg)	D_1 (m)	D_2 (m)	L (m)	L_2 (m)	L_3 (m)	L_4 (m)
Prototype	12000	4.50	1.200	3.25	10	5.875	3.00
Model	6.0	0.36	0.096	0.26	0.8	0.47	0.24

Table 2. Results of physical model experiment and numerical calculation

	Wave Height (m)	Wave Cycle (s)	Water Depth (m)	Rope-Retraction Force (N)	Damping Force (N)	Acquisition Power (W)	Collection Efficiency (%)
Model Experiment	0.14	2.06	1.08	58.8	64.8	3.95	23.7
Method 1	0.14	2.06	1.08	58.8	64.8	3.15	18.9
Method 2	0.14	2.06	1.08	58.8	64.8	4.15	24.9

coil spring providing rope retraction force, and the other end is connected with the rope. The other end of the rope goes around the two guide wheels at the bottom of the wave tank, passes through the guide rod and the duct, and is connected to the force sensor installed inside the floating body. Among them, the force sensor is used to measure the rope tension, some rollers are installed between the duct and the guide rod, the guide rod is connected with the ball hinge, and the guide rod is fixedly connected with the floating body. On the right side of the synchronous pulley is a magnetic particle damper, which is used to simulate the damping of PTO system, and a one-way

bearing is installed between the synchronous pulley and the synchronous pulley shaft to achieve the one-way acquisition feature of the wave energy device.

The rope retraction force of the physical model device and the damping force of PTO system are provided by the constant force coil spring and magnetic powder damper respectively. The constant retraction rope force provided by constant force coil spring simulates the characteristics of prototype with approximately constant retraction chain force. The magnitude of the damping force provided by the magnetic particle damper is controlled by the magnitude of the current of magnetic particle damper. The physical model experiment is based on the similarity principle of fluid mechanics. The scale ratio between the prototype and physical model is 12.5. The main parameters of them are shown in Table 1, and the meaning of the dimension parameters in Table 1 is shown in Fig. 10.

4.2 Comparison between Experimental Results and Calculation Results

The parameters and results of the physical model experiment are shown in Table 2. Under this condition, the first-level average collection power calculated by method 1 and method 2 are 3.15W and 4.15W respectively, and the relative errors are 20.3% and 5.06% respectively, compared with the experimental result 3.95W. From Fig. 11 to Fig. 13, it can be seen that the instantaneous hydrodynamic responses calculating with numerical calculation model established in this paper from 0 to 10 seconds are in good agreement with the experimental results of the physical model, and the method 2 has more accurate calculation results.

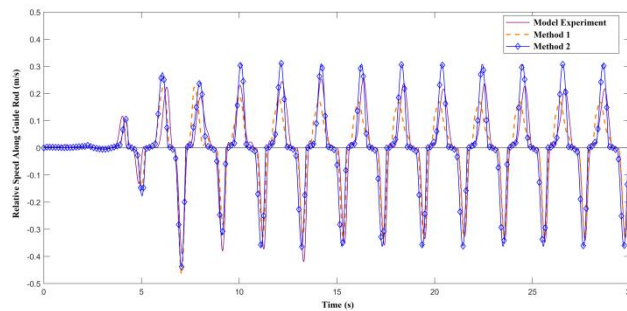


Fig. 11 Comparison figure of the relative velocity of the floating body along the guide rod.

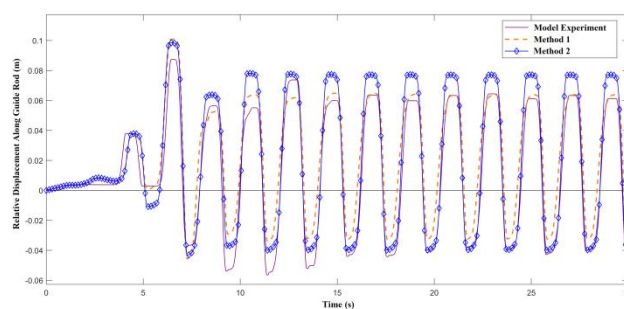


Fig. 12 Comparison figure of the relative displacement of the floating body along the guide rod.

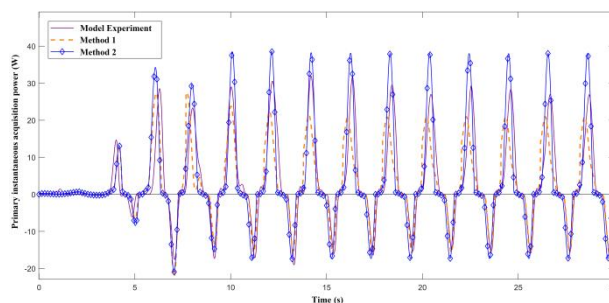


Fig. 13 Comparison figure of primary instantaneous collection power of the physical model device.

5. Conclusion

Buoy-chain-sprocket wave energy collection device whose chain-sprocket mechanism is used to collect wave energy, has the advantages of simple structure, good reliability, low operation and maintenance cost, with the characteristic of one-way wave energy collection. On basis of linear potential flow theory, Cummins method is used to establish the hydrodynamic response calculation model of buoy-chain-sprocket wave energy collection device. Subsequently, the calculation method of hydrodynamic performance of the device is proposed. In order to further improve the calculation accuracy, the influence of the frequency-domain wave-exciting force on the hydrodynamic response of buoy-chain-sprocket wave energy collection device is explored in this paper by using the average draft depth and variable draft depth of the floating body respectively. Then, the experimental results of the physical model are used as the inspection standard, which verifies that the calculation method of buoy-chain-sprocket wave energy collection device, with variable draft depth to calculate frequency-domain wave- exciting force, has a better reliability.

Acknowledgment

This work was supported by the National Marine Renewable Energy Project of China whose grant number is GHME2011BL02, and Key Technology Research and Development Program of Shandong Province whose grant number is 2018GHY115024.

References

- [1] A. Clément, P. McCullen, A. Falcão, A. Fiorentino, F. Gardner, K. Hammarlund, et al., “Wave energy in Europe: current status and perspectives,” *Renewable Sustainable Energy Rev.*, vol. 6, Oct. 2002, pp. 405-431, doi:10.1016/S1364-0321(02)00009-6.
- [2] J. Falnes, “A review of wave-energy extraction,” *Mar. struct.*, vol. 20, Oct. 2007, pp. 185-201, doi:10.1016/j.marstruc.2007.09.001.
- [3] F. O. António, “Wave energy utilization: A review of the technologies,” *Renewable Sustainable Energy Rev.*, vol. 14, Apr. 2010, pp. 899-918, doi:10.1016/j.rser.2009.11.003.
- [4] J. Burhanudin, A. S. A. Hasim, A. M. Ishak, J. Burhanudin and S. M. F. B. S. M. Dardin, “A Review of Power Electronics for Nearshore Wave Energy Converter Applications,” *IEEE Access*, vol. 10, Feb. 2022, pp. 16670-16680, doi:10.1109/ACCESS.2022.3148319.
- [5] W. Sheng, “Wave energy conversion and hydrodynamics modelling technologies: A review,” *Renewable and Sustainable Energy Rev.*, vol. 109, Jul. 2019, pp. 482-498, doi:10.1016/j.rser.2019.04.030.
- [6] Zhu, L.S., Zhu, Z.L., Ji, F.D., “An oscillating buoy wave energy capture system,” *China Patent CN110594082A*, Sep. 24, 2019.
- [7] Zhu, L.S., Zhu, Z.L., Ji, F.D., “Buoy-chain-sprocket wave energy capture system with a vacuum cylinder to recover chain,” *China Patent CN109973289A*, Mar. 14, 2019.
- [8] W. E. Cummins, “The impulse response function and ship motions,” *Schiffstechnik*, vol. 9, Oct. 1962, pp. 101-109.
- [9] R. W. Yeung, “Added mass and damping of a vertical cylinder in finite-depth waters,” *Appl. Ocean Res.*, vol. 3, Jul. 1981, pp. 119-133, doi:10.1016/0141-1187(81)90101-2.
- [10] C. J. R. Garrett, “Wave forces on a circular dock,” *J. Fluid Mech.*, vol. 46, Mar. 2006, pp. 129-139, doi:10.1017/S0022112071000430.